Sloppiness and Action Confinement in Cell State Transitions: Are Single Cells Sloppy?

Junda Ying[1*], Yuxuan Wang[2*], He Xiao[1,2*], Miao Huang[1,2], Lei Zhang[5], Weikang Wang[3,4]

[1]School of Mathematical Sciences, Peking University, Beijing 100871, China

[2]Center for Data Science, Peking University, Beijing 100871, China

[3]Institute of Theoretical Physics, Chinese Academy of Sciences, Beijing 100190, China

[4] School of Physical Sciences, University of Chinese Academy of Sciences, Beijing 100049, China

[5]Beijing International Center for Mathematical Research, Center for Quantitative Biology, Center for Machine Learning Research, Peking University, Beijing 100871, China.

*Equal contribution

Email: wangwk@itp.ac.cn, zhangl@math.pku.edu.cn

Abstract

Single-cell dynamics during cell state transitions are highly confined, ensuring precise control. This confinement can be described using low-dimensional manifolds. Leveraging information geometry, we developed a method to quantify cell state transition manifolds using single-cell RNA sequencing data. With this approach, each single cell is represented as a multivariate Gaussian distribution and is associated with a Fisher information matrix.

We analyzed variations in the Fisher information matrix and its eigenvalue spectrum during cell state transitions. Our results reveal pronounced sloppiness in single cells, where cell state is sensitive to only a few specific combinations of parameters. Importantly, the degree of sloppiness fluctuates during cell state transitions. We found that critical transitions are associated with changes in the so-called stiff parameters. Notably, parameters identified as stiff exhibit low velocities and minimal fluctuations, whereas sloppy parameters display higher velocities and

larger fluctuations. These findings indicate that cells fine-tune sensitive directions with caution while permitting greater flexibility along sloppy directions, revealing a principle of least action confining the paths taken during state transitions. During transitional stages, fluctuations and velocities increase were observed on stiff parameters, reflecting enhanced dynamical activity as cells navigate through critical regions of the manifold.

Thus, we propose a new framework for analyzing single-cell dynamics. The low dimensionality of cell state transitions is characterized through sloppiness analysis, while changes in the Fisher information spectrum reveal shifts in cell dynamic modes.

Introduction

Quantification of single-cell transition manifolds is crucial for understanding cellular dynamics. Waddington introduced the well-known landscape metaphor to illustrate embryonic development (1). With the advent of high-throughput techniques, particularly single-cell RNA sequencing, it has become possible to quantify Waddington landscapes within high-dimensional gene spaces (2, 3, 4, 5). However, this quantification and visualization often depend on low-dimensional embeddings. Current embedding methods, such as UMAP or diffusion maps, tend to distort local distance metrics, especially when projected into two dimensions (6). In our previous study, we developed a method named SCIM (Single Cell Information Manifolds) that is based on information geometry(7). This method represents single cell states as probability density functions and allows for the quantification of single-cell manifolds from the perspective of intrinsic geometry based on Fisher information metric. And we demonstrated that cell dynamics are linked to the geometric properties of these manifolds.

Fisher information can be used to quantify the sensitivity of probability density function to control parameters. With Fisher information, one can define the sloppiness and stiffness of parameters or parameter combination in fitting large scale models. Sloppiness refers to the phenomenon in multi-parameter models where only a few parameter combinations significantly influence the model when fitting to collective behaviors. The model is particularly sensitive to these combinations, which are referred to as stiff parameters. The remaining parameters, in contrast, are considered sloppy parameters (8, 9). The strength of the impact on the system caused by changes in the parameter combinations corresponding to the eigen-directions of the Fisher information is quantified by their eigenvalues. If one Fisher information matrix has only a

few large eigenvalues while the others are significantly smaller, the system is said to be "sloppy". Thus the model manifold of predictions, whose coordinates are model parameters, form a hyper-ribbon geometry (10, 11). The widths of the model manifold follow a geometric spread, roughly even in log scale or power law decay (8, 9, 12).

Cell state transitions (CST) usually involve the regulation of different genes at various stages. If we consider development as an adaptation process, the system adjusts its parameters to enhance fitness (13). This process resembles an online fitting of a model to a changing environment. Cells activate different genes and modulate their expression levels to adapt to external signals (14, 15, 16). These genes function as parameters, and their sensitivity varies during CST. Different genes exhibit distinct levels of Fisher information during these transitions (7). In this work, we treated cells as online fitting models and analyzed their sloppiness and stiffness.

Sloppiness analysis has been applied to analyzing biological systems like neuroscience and system biology (17, 18). For instance, Panas et al. fitted the network activity of cultured rat hippocampal neurons using pairwise maximum entropy model and discovered that the model is sloppy. They also found that neurons with sloppy parameters exhibited faster and larger fluctuations compared to those associated with sensitive parameters (19). Similarly, Adrian Ponce-Alvarez et al. investigated the neural population activity in the auditory cortex of anesthetized rats and found that stimulus-evoked activity predominantly occurs along sloppy dimensions, while cortical state transitions progress along stiff directions (20). Gutenkunst et al. found that systems biology models show sloppy spectrums of sensitivities (21).

As a specific type of Riemannian metric, Fisher information can be used to quantify the length and action of transition path on the manifolds of CST. Crooks utilized information length on the information manifold to interpret thermodynamic length (22). Eun-jin Kim analyzed information change in non-equilibrium processes using information length (23). One can calculate information velocity with Fisher information metric and parameter velocity which reflects the variation rate of probability distribution (22, 23).The integration of square of information velocity along a path is defined as action on the information manifolds. In analytical mechanics, least action is a general principle to summarize the dynamics of a systems into a Lagrangian, from which the dynamics equation can be deduced. The least action principle adds a universal

constrain on classical dynamics. People may wonder if this principle can be extended to cell dynamics. The inference of RNA velocity invoked the studies on action of transition path in single cell RNA sequencing data. Qiu et al. developed a method for calculating least action paths using reconstructed vector fields from single-cell RNA sequencing data (24). Zhu et al. introduced a method for calculating landscape and flux from reconstructed vector fields and confirmed Wang's conclusions that least action paths do not necessarily follow the landscape's gradient when there is a non-zero curl flux (25, 26). Transition paths can be readily quantified with information manifold from the perspective of intrinsic geometry. Analyzing the stiffness and sloppiness of parameters along the transition path can reveal how single cell dynamics is controlled in CST. For instance, stiff parameters and sloppy parameters are related with plasticity and robustness of cell state and cell function respectively (18, 20).

Identifying stiff and sloppy parameters at different stages is crucial for comprehending the underlying regulatory mechanisms of CSTs. However, there are few studies analyzing single-cell dynamics from this perspective. In this work, we utilize the single-cell information manifold to investigate the sloppiness of the dynamic fitting processes in cellular systems. Our findings reveal that cellular systems exhibit significant sloppiness. And stiff parameters increase as cells approach transition states. Notably, the cell system tends to minimize action on information manifolds.

Results

Analyzing sloppiness of single cell with spectrum of Fisher information matrix

We presented a framework for analyzing the single cell dynamics through single cell's FIM. In this work, we mapped each cell to a multi-dimensional Gaussian distribution (Fig. 1a) (Methods). We got the FIM of each distribution and regarded the FIM as metric in statistical manifold (Fig. 1b). Through this Gaussian embedding, we fulfilled fitting a special model about the single cell data. For each single cell, it is fitted with a specific set of parameters which are (μ, σ) in Gaussian distributions. Intuitively, the Gaussian distributions capture the uncertainty or neighborhood diversity of single cells. With the fitted model, we can analyze the eigen-spectrums of FIM of different single cells (Fig. 1c). The spectrum analysis reveals the sloppiness of single cell. Large eigen values indicate stiff parameters, indicating the potential critical

regulation in the cells and the eigen-vectors correspond to large dynamic behavior directions. For each cell type, the distribution of eigen values and eigen vectors can reveal the heterogeneity of single cell.

Beyond analyzing static spectrum, we focused on the variation of eigen-spectrum in CST. Through constructing transition graph based on RNA velocity, the averaged transition path of CST can be estimated. The variation of Fisher information along the transition path can reveal the variation of parameter space beyond dynamics space.

Specifically, increase of large eigen values of FIM indicates a cell becomes sensitive to more factors, which is associate with cell plasticity (Fig. 1c). And these factors can be analyzed by examining the corresponding eigenvectors. Through coordinate transformation, Fisher information of every gene especially the transcriptional factor can be defined (Fig. 1d left). The distribution of genes' Fisher information change along the transition path (Fig. 1d right), which can be used to analyze the important marker genes and regulatory genes at different stage of transition.

With Fisher metric and parameter velocity, the information velocity and action on the information manifold along the transition path can be analyzed. This analysis can be simply extended to analyzing the relation between parameter's Fisher information and parameter velocity (Fig. 1e).

Spectrum analysis of Fisher information matrix reveals sloppiness of CST

Here we applied our method on several single cell RNA sequencing datasets including zebrafish pigmentation (27) and dentate gyrus neurogenesis (28). During zebrafish pigmentation, proliferating progenitors differentiate into pigment progenitors and Schwann cell precursors, ultimately forming melanophores, xanthophores, and Schwann cells, representing a tri-fate differentiation process (Fig. 2a). The steady states consist of the initial phenotype (proliferating progenitors) and the terminal phenotypes (melanophores, xanthophores, and Schwann cells), while the transient states include pigment progenitors and Schwann cell precursors. Pigment progenitors serve as a branch point, differentiating into multiple pigment cell types, while Schwann cell precursors exclusively develop into Schwann cells, representing a single-lineage critical transition. Coase Ricci curvature (CRC) results indicate that low-curvature regions

precisely demarcate the transient states, while high-curvature regions correspond to steady states (Fig. S1a).

Dentate gyrus neurogenesis involves differentiation processes of multiple cell types. For comparison with CST with multiple lineages like zebrafish pigmentation. Here we focused on the transition from radial glia to granule cells through neuroblasts, which is a single-lineage CST process (Fig. 2b). The critical transition occurs at the transient state, i.e neuroblasts. CRC results show that low-curvature regions precisely demarcate the transient state (Neuroblasts), while high-curvature regions correspond to steady states (radial glia and granule cells) (Fig. S1b).

We transformed the single cells into multi-variate Gaussian distributions with diagonal covariances for simplicity. We first investigate the spectrum of each single cell with FIM in $(\boldsymbol{\mu}, \boldsymbol{\sigma})$ coordinates. The Fisher information of Gaussian embeddings with diagonal covariances can be written analytically. For 1-D Gaussian distribution, the Fisher information of μ and σ are $\frac{1}{\sigma^2}$ and $\frac{2}{\sigma^2}$ respectively (29, 30). And the Fisher information matrix G of a L-dimensional diagonal Gaussian distribution is:

$$G = diag(\frac{1}{\sigma_1^2}, \frac{2}{\sigma_1^2}, \dots, \frac{1}{\sigma_l^2}, \frac{2}{\sigma_l^2}, \dots, \frac{1}{\sigma_L^2}, \frac{2}{\sigma_L^2})$$

Since the Fisher information of μ is one half of that of corresponding σ, one can only analyze the Fisher information of $\boldsymbol{\mu}$ or $\boldsymbol{\sigma}$ in practice. We found that Fisher information can be used to characterize cell type (Fig. 2c,d). For instance, the proliferating progenitors and Schwann cell show significantly different Fisher information values especially that dimension with largest Fisher information are different (Fig. 2c). In neurogenesis the neuroblast (neuroblast2) show apparent signature of transition. As transition proceeds, cell types like radial glia and neuronal intermediate progenitor (nIPCs) exhibit largest Fisher information in the first row and cell types like immature granule cells and granule cells have largest Fisher information in the ninth row. But in neuroblast2 some cells have largest Fisher information in the first row and some cells have largest Fisher information in the ninth row, indicating transitional role of neuroblast2 (Fig. 2d). But the FIM obtained from Gaussian embedding directly suffers from several disadvantages. One is the Gaussian embedding is derived from training a neural network where there is randomness. Hence interpreting sloppiness with Fisher information of $(\boldsymbol{\mu}, \boldsymbol{\sigma})$ depends on the

embedding results (7). The other is that $(\boldsymbol{\mu}, \boldsymbol{\sigma})$ lack biological meanings. Fortunately, geometry properties of the single cell manifold like curvature are invariant under different parameterization $(\boldsymbol{\mu}, \boldsymbol{\sigma})$. As different $(\boldsymbol{\mu}, \boldsymbol{\sigma})$ can keep the geometry of the single cell manifold, they can be treated as coordinate transformation, i.e., different $(\boldsymbol{\mu}, \boldsymbol{\sigma})$ represent different coordinate systems. We utilize the idea of coordinate transformation and transform $(\boldsymbol{\mu}, \boldsymbol{\sigma})$ to gene modules like eigengene and Hotspot (methods). Eigengene represents the PC1 of gene modules identified through gene correlation clustering, while Hotspot modules are generated by identifying genes that share informative co-variation and similarity in proximal cells. The FIMs in the transformed coordinates are not necessarily diagonal and we computed the eigen spectrums. The mean (Fig. 2e,f) and distribution (Fig. S2a,b) of eigenvalues of each order (normalized by the 1st eigenvalue) were shown per cell type. It can be observed that, on a logarithmic scale, the eigenvalues of the Fisher information are sparsely distributed with significant magnitude differences on all these datasets. Only a few parameter combinations are stiff, while other parameter combinations are sloppy. This indicates that the CPT system is "sloppy," consistent with the widely accepted assumption of low intrinsic dimension. And the number of stiff parameters is less than embedding dimensionality. The spectrums of Hotspot modules exhibit similar sloppiness (Fig. S2c,d). These results are consistent with the eigen spectrum of FIM in complex model fitting (8, 9, 21). Especially the results of sloppiness are irrelevant with the hyperparameter of latent embedding *L*.

Spectrum of Fisher information at transitory stages

We further separate the whole cell population into different clusters with PAGA (Fig. 2g,h) and investigate the dominant parameter combinations in each cluster (31). The system is dominated by the stiff parameters defined by the eigenvectors of FIM corresponding to similar large eigenvalues. More stiff parameters indicate a higher degree of freedom and high cell plasticity. And the stiff directions may correspond to different regulatory or functional modules in gene networks. The violin plot of eigenvalues of each order under Eigengene coordinates were shown for each PAGA cluster (Fig. 2i,j). In both zebrafish pigmentation with multi-lineages and dentate gyrus neurogenesis with single lineage, the gap between the first and second eigenvalue significantly shrink near the cell stages with higher degree of freedom. Since eigengene and Hotspot modules both reflect the properties of gene regulatory networks (32, 33), the ratio of

eigenvalue could be now interpreted biologically. In single-lineage data, the stiffness of more parameter combinations increased near critical transition, indicating more active gene interactions and dominant gene module switch during cell phenotype transition. In multi-lineage data, the gap between the first two eigenvalues becomes smaller around the undifferentiated clusters s and sometimes, even an overlap could be observed in the violin plot. These imply the dominant gene module selection during cell fate decision, where many genes were stiff to the system due to undecided cell fate, while only some of them would be dominant during the following specific differentiation process where the cell fate was partially decided. These results are robust, similar phenomena can also be observed in FIMs of eigengene and Hotspot with different parameter settings (Fig. S3, Fig. S4).

We also examined the ratio between the second and first eigenvalue of each cell under Hotspot coordinates (Fig. 2k,l). Consistent to the violin results, the ratios peak at the same region. This indicates that biological system is sloppy under single-cell resolution, and the switch and selection of stiff parameter combinations are single-cell-wise. The results are consistent in FIMs of eigengene and Hotspot with different parameter settings (Fig. S5, Fig. S6), and the analysis of pancreatic endocrinogenesis dataset is shown in Fig. S8.

Variation of genes Fisher information in CST

We have already discussed the sloppiness of the CPT system on collective coordinates like gene modules. Furthermore, we can extend this analysis to gene levels. By transforming the Fisher information matrices from the latent embedding space to the gene expression space (Methods), we obtained gene-by-gene Fisher information matrices. Each off-diagonal element of this matrix represents the Fisher information for a corresponding gene pair, while the diagonal elements represent the Fisher information for individual genes. As shown in Fig. 3a, the average values and variances of normalized Fisher information of selected genes varies across different cell types in zebrafish pigmentation, indicating the variation of genes' stiffness in different cell types.

Next, we examined the variation of distribution of genes' Fisher information in CST. Though single cell data are generally snap-shot data without dynamics information, the transition path could still be inferred based on prior knowledge and reasonable assumptions. Based on RNA velocity, we calculated the averaged transition paths in zebrafish pigmentation (Methods)(16).

The averaged transition path is discretized into multiple reaction coordinates (RC) (Fig. 3b, center). RC is a set of points equally distributed along the transition path, and the multi-dimensional state space was divided into Voronoi grids(16, 31). Each cell's RC value was assigned based on the Voronoi grid it resides in. In the context of cell phenotypic transitions, a RC can be conceptually related to a pseudo-time trajectory in the single cell genomics field(32, 33).

We quantified sensitivity using the distribution of genes' Fisher information of neighboring cell of the RCs along transition paths. The Fisher information of each gene was normalized by its maximum Fisher information in all the cells (Fig. 3b). Here we showed the paths that transitions from proliferating progenitors to melanophores, and Schwann cells, respectively. For instance, the Fisher information distribution of rrm2 becomes dispersive indicating rrm2 become stiffer when transiting into Schwann cell. The path from proliferating progenitors to xanthophores can be found in Fig. S9.

We calculated genes' average Fisher information in the corresponding Voronoi grid of each RC along the transition path. We found that the average Fisher information distribution varies along the transition path, but exhibit similar dynamic patterns. As shown in Fig. 3c, the distributions of relative Fisher information at most RCs are close to bimodal distribution, which indicate that there is a small proportion of genes with high Fisher information. We used a two-component Gaussian mixture model (GMM) to fit each distribution (Fig. 3c) and the separation between the two components reach a peak during CST (Fig. 3d). The positions of peaks locate around the transition cell states. In the Zebrafish pigmentation data, the peaks are near pigment progenitors, and Schwann cell precursors near the transition point, which have higher instability, compared to the terminally differentiated cell types (Fig. S10). This indicates that at the transitory stage, cells are sensitive to the expression levels of more genes. Not only bifurcations, the switching of dominant gene modules near transitory stage can also cause cells to become locally sensitive to the expression levels of more genes. A noticeable increase in separation is also observed at the transitory stage in the single-lineage dentate gyrus data (Fig. 3e,f and Fig. S11).

Similarly, we calculated the distributions of Hotspot modules' Fisher information (Fig. 3g) along the transition path from proliferating progenitor to melanophore and also observed the shift of distributions of Fisher information.

Then we performed gene ontology (GO) enrichment analysis on the genes whose Fisher information show large variance in CST (Fig. 3h). And found that these genes are related with several critical biological pathways correlated to zebrafish pigmentation and Schwann cell development including tyrosine metabolism, Notch signaling, and melanogenesis.

Stiff direction increases at multi-lineage transitory stages

The variation of FIM eigenvalue spectrum reveals that more parameters become stiff when cell approaching the transitory stage. Following this, we further examine the variation of FIM eigenvectors. Specifically, we examined the eigenvectors corresponds to the first several largest eigen value of FIM. These vectors represent the stiffest parameter combinations. For short, we call this these eigenvectors stiff directions. Through analyzing the stiff direction under different biologically meaningful module coordinates and within different cell types, we can obtain some hints on how CST is regulated by underlying gene regulator networks. For example, we analyzed the distribution of 1st stiff direction of eigengene FIM in each cell type (Fig. 4a). As the stiff direction is a multi-dimensional vector that can be in two opposite orientations. The orientation would largely affect the distance value. Here we first adjusted the sign of directions by solving an integer programming problem with Gurobi algorithm (Fig. S13) (Methods). Then the correlation distance matrix of the aligned stiff directions of the pancreatic endocinogenesis dataset with eigengene coordinate (Fig. 4a inserted heatmap). By learning a mapping between the stiff direction and the embedding coordinates like UMAP (Methods), the vector plot of stiff directions of each cell type are show with the scatter plot on the embedding coordinates (Fig. 4a, inserted arrow bundles). We can see that the distribution of 1st stiff direction is quite narrow at the starting point and end point of cell differentiation, but it becomes dispersive at the branch point.

Furthermore, we previously observed that the relative increase of 2nd largest eigenvalue of FIM at the transitory stage. The relative change in eigenvalue may lead to changes in the corresponding eigenvectors. Therefore, we examined the inner product of the second and first stiff directions in each cell type (Fig. 4b). In Ngn3-low progenitor cells, the inner product is low. But for Fev+ and glucagon-producing α-cell, there are non-diagonal blocks with value close to 1 indicating that the 2nd stiff direction (corresponding to the row) of one group are similar to the 1st

stiff direction (corresponding to the column) of another group. Based on the inner product of stiff directions, we can separate the Fev+ cell types can be seperated into three clusters (Fev+_1, Fev+_2, Fev+_3). The most obvious result is that the 1st and 2nd stiff directions in Fev+_1 cells are approximately 2nd and 1st stiff directions in Fev+_2 cells respectively. This means that stiff directions of cells in those cell types switch between the two types of vectors. Due to the randomness and data quality, this matching is rough, but it explains the rationality of multiple clusters of the 1st stiff directions in these cell types.

Finally, we compared the components in these stiff directions in different coordinates (Fig. 4c). The distribution of stiff directions in cells at the branch point is relatively dispersed across the components, while it is more concentrated at the initial and final states. Different branches exhibit different component distributions; for example, glucagon-producing α-cell is higher in eigengene-3 and lower in eigengene-1, while glucagon-producing β-cell shows the opposite. The variation of components distribution reveals the variation of stiff directions in CST. We performed the same analyses with Hotspot coordinate and obtained similar results on the distribution of stiff directions (Fig. S15).

We also analyzed the stiff directions along the transition path discretized by RC (Fig. 4d). For transition from proliferating progenitors to Schwann cells in zebrafish pigmentation, the correlation distance values between 1st stiff direction at RC2 span large range while the distance values at RC5 and RC8 are almost equal 1 (Fig.4d inserted heatmap). And distribution of 1st stiff direction on UMAP at RC2 is more dispersive than those at RC5 and RC8 (Fig. 4d inserted heatmap). The inner product of the second and first stiff directions reveals that the neighboring cells of RC2 can be separated into three groups, while the other two only exhibit one group (Fig. 4e), reflecting the heterogeneity at RC2. We also examined the distribution of components in 1st direction along the RCs (Fig. 4f). Several eigengene modules show dispersive distributions at RC1 and RC2, but keep either low value (module 17) or high value (module 27) at the following RCs. In zebrafish pigmentation, neighboring cells of RC1and RC2 are mainly proliferating genitor cells, which can different into different cell types including Schwann cell and Melanophores. Different from pancreatic endocrinogenesis whose stiff directions become dispersive at the cell type like Fev+ around the branch point, the dispersive stiff directions at proliferating genitors indicate that cells probably adopt different mechanisms of making cell fate

decision. In zebrafish pigmentation, the timing of decision making is earlier than that in pancreatic endocrinogenesis. We also analyzed the transitions to Melanophores and Xanthophores (Fig. S16).

Fluctuations of stiff and sloppy parameters

CST not only relates to changes in the Fisher information of parameters, but also involves variation of the parameters themselves. In this section, we investigate the fluctuation properties of stiff and sloppy parameters along the transition paths (Fig. 5a). The magnitude of fluctuations is quantified by the squared coefficient of variation (CV^2; see Methods).

Firstly, we found stiff parameter exhibits smaller fluctuations than sloppy parameter in different transition processes including dentate gyrus neurogenesis (Fig. 5b left), pancreatic endocrinogenesis (Fig. 5b middle) and zebrafish pigmentation (Fig. 5b right), as reflected by their lower CV^2 values at the neighborhood of each RC. Secondly, along the RC of transition paths, the CV^2 of stiff parameters show a pronounced negative correlation with their Fisher information (Fig. 5c). These findings are robust (Fig. S17) and are consistently reproduced across other branches in pancreatic endocrinogenesis and zebrafish pigmentation datasets (Fig. S18).

Since the Fisher information characterizes the sensitivity of a parameter, these results implied that stiff parameters fluctuate less, and that the magnitude of fluctuations further decreases as parameter sensitivity increases. Biologically, such stiff parameters may correspond to key genes or critical regulatory mechanisms governing cell sate transitions. Small perturbations in these stiff parameters can lead to substantial changes in cell state, and therefore the system tends to cautious regulate them, giving rise to the reduced fluctuations observed in our analysis.

Least action principle in CPT

Following analyses of the parameter fluctuations, we further examined the velocities of stiff and sloppy parameters in each single cell. We calculated the parameter velocity of $(\boldsymbol{\mu}, \boldsymbol{\sigma})$ based RNA velocity (Methods) and found that there is an obvious negative correspondence between Fisher information and parameter velocity (Fig. 6a-c). For instance, the Fisher information of σ_1 is low at the initial stage and high at the final stage in dentate gyrus neurogenesis, but its parameter velocity exhibits opposite the distribution (Fig. 6a).

And we performed a more detailed analysis along the transition paths discretized with RC (Fig. 6d-f). The average Fisher information and parameter velocity of each RC's neighboring cells are plotted. There are two major common characteristics can be obtained from this analysis. One is that the parameter velocity is low when Fisher information is high, which indicate that the stiff parameters do not show fast variation in CST. The other is that the parameter velocity can fluctuate when Fisher information is low. For instance, for σ_2 in the pancreatic endocrinogenesis dataset, while its Fisher information remains low across all reaction coordinate (RC) points, its velocity is fluctuating, being high in the first half of the RC path and low in the second half (Fig. 6e). These results are consistent with the results that the stiff parameters have lower fluctuations (Fig. 5b).

We can interpret these results from the perspective of action on the Riemann manifold. Consider the action along the transition path

$$J = \int dt\, v^i v^j g_{ij},$$

which is the integral of the square of information velocity along the path. This action has a lower bound related to the length of the path:

$$J \geq \frac{L^2}{T},$$

where

$$L = \int dt \sqrt{v^i v^j g_{ij}} = \int dl$$

is the length of the path, and

$$T = \int dt$$

is the total time.

The paths which minimize this action to the lower bound are the geodesics on the manifold, and their parametrization by time t satisfies

$$v^i v^j g_{ij} = constant$$

along the paths, so the corresponding time parameter t is proportional to the length l along the paths. Information velocity $\sqrt{v^i v^j g_{ij}}$ represents the variation rate of probability distribution, i.e, cell state.

From the definition, we can see that to minimize the action, which is equivalent to keep the information velocity constant along the path, the velocity and metric must vary in a complementary way: g_{ij} must be small where $v^i v^j$ is large, and vice versa. This imposed a constrain on the parameter velocity in turn. For sloppy parameters whose influence on information velocity is low, their parameter velocities are less confined. But for those stiff parameters, their parameter velocity confined to low levels because variation of stiff parameters can significantly change cell state. Hence, we can draw the conclusion that cells tend to be sloppy, that is cells tend to minimize the information velocity. And when a parameter's Fisher information varies, its parameter velocity usually varies with the opposite trend in transition states.

In CST processes, the situation is complex. As we have discovered that the information velocity transiently increases at the transitory stage in CST from one cell state to another state. The increase of information velocity reflects the fast variation of cell state. In CST with branching of different lineages, the trend of information velocity is more complicated because it involves the regulation of different stiff parameters, or interaction between different GRN modules. Nevertheless, these results suggest that CPT process progress in a way that tries to minimize the action in most time, which may be related to the saving of energy; but around at transitory stage, this principle is not satisfied, since the cell state is undergoing drastic changes and is very sensitive to external stimulations, so much energy is consumed. From the perspective of control, the cell would rather tune the sloppy parameters to avoid state transition unless state transition is inevitable.

Discussion

People commonly use bifurcation or potential landscape for illustrating different types of CSTs. But analyzing the bifurcation of high-dimension system is challenging as it usually relies on clear definition of cell dynamics. And the landscape requires on definition of ambient space like UMAP which may distort the geometry structure of data. The variation of FIM provide a new

perspective for analyzing complex state transition. Through transforming single cell into Gaussian distributions and quantifying FIM, the systems' dynamics space can be depicted geometrically with the spectral structure of FIM. Other than analyzing CST in the dynamics space, we mapped the cell dynamics in CST to parameter space (Fig. 7) and characterized CST processes with variation of FIM spectrum especially the switch of stiff parameters. It should be noted that Fisher information is not directly related to causal relation. But we can still obtain acquire knowledge on system control through mapping onto parameter space. In our analyses, we use linear decomposition of FIM to analyze the variation of stiff directions. However, the stiff directions could be certain non-linear combinations of individual parameters. Non-linear method for analyzing sloppiness from FIM could be further developed.

Due to the remarkable precision, CSTs are generally believed to be confined to lower-dimensional manifolds. In this study, we used the concept of sloppiness and the principle of least action to explore the low dimensionality of CST. Despite the inherently high-dimensional and complex nature of single cells, which are governed by numerous parameters, our analysis reveals that cell states are predominantly sensitive to only a few parameter combinations. In other words, the control parameters of CPT are far fewer than the dimensions of the gene expression space. Interestingly, the number of stiff parameter combinations shows an increasing trend during transitions, compared to meta-stable cell states. This indicates an increase in stiff parameters during transitions, particularly when cells undergo branching processes. The augmentation of stiff parameters corresponds to an increase in dynamic modes within the behavioral space.

In this work, we transformed the cell state into Gaussian distributions and analyzed the sloppiness of the parameters. To solve the problem that the parameters of Gaussian embeddings, i.e. mean and standard deviation, lack biological meaning, we performed coordinate transformation from the geometric perspective. The transformed coordinates serve as new parameter combinations. In our analyses, the new parameter sets are usually chosen as collective variables like eigengene and Hotspot modules. These collective variables reflect the organization of gene regulatory networks. In CST, gene regulation networks are likely dynamical(14, 15). The variation of regulation strength directs the critical transition or bifurcation. However, those variables cannot capture the direction interaction between gene modules or regulatory strength among genes. The sloppiness of gene regulation weights requires

more accurate inference of gene regulatory network. In the gene level, a gene is "stiff" means that it has a significant impact on biological processes and plays a dominant role. Such genes are more likely to interact with other genes, resulting in larger non-diagonal elements of the Fisher information corresponding to that gene pair. But this is not a formal definition on Fisher information of gene interaction. A potential way would be inferring gene regulatory network and calculate the Fisher information of regulatory strength between genes.

Figures

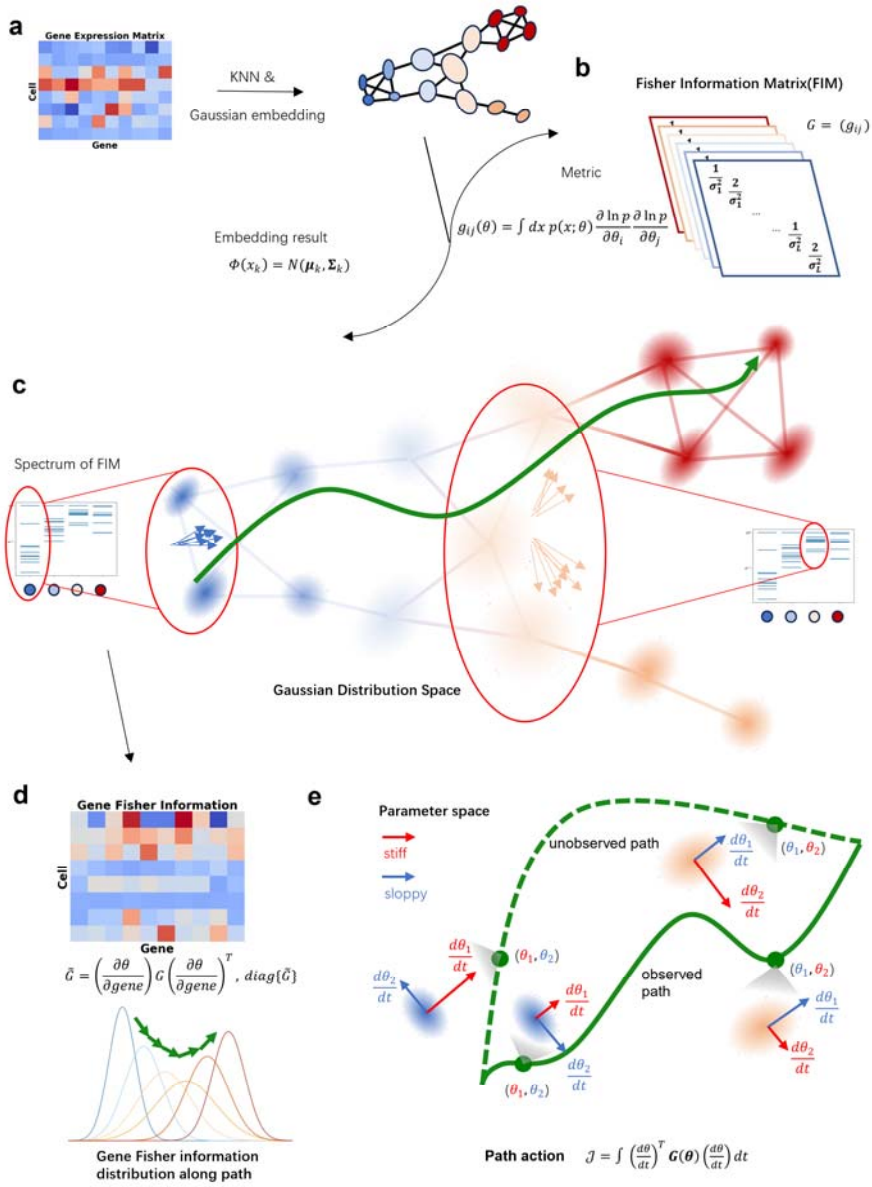

Figure 1. Analyzing single cell state transition with spectrum of FIM.

(a) Through building KNN cell graph and Gaussian embedding, each cell in single cell RNA sequencing data is mapped into a multi-variate Gaussian distribution with SCIM.

(b) Each single cell is endowed with a Fisher information matrix which is regarded as the Riemannian metric of the cell state transition manifold.

(c) Each shadowed ellipse on the embedding space represents a Gaussian distribution of a cell embedding, and the connections on the graph are derived from KNN. The spectrum

of FIM's eigenvalues (blue bars) of different cell types are shown in the box. The arrow bundles in the red circles represent the largest eigenvalue's eigenvectors of all cells in the corresponding cluster. The green line represents an averaged smooth path for cell state transition.

(d) Using distribution of genes' Fisher information to evaluate the possible regulation mechanism in cell state transition. Each curve represents the probability density of Fisher information across all genes on average within the corresponding cell type (represented by color).

(e) Action confinement on corresponding parameter Fisher information and parameter velocity along the transition paths. Each point represents a Gaussian distribution characterized by parameters $(\theta_1,\ \theta_2)$, with local ellipses indicating the stiff (red) and sloppy (blue) directions in parameter space. Arrow length indicates magnitude of parameter velocity. Solid green curve represents the observed path with minimized action. The unobserved path with larger action (dashed green curve) may have larger velocities along stiff directions.

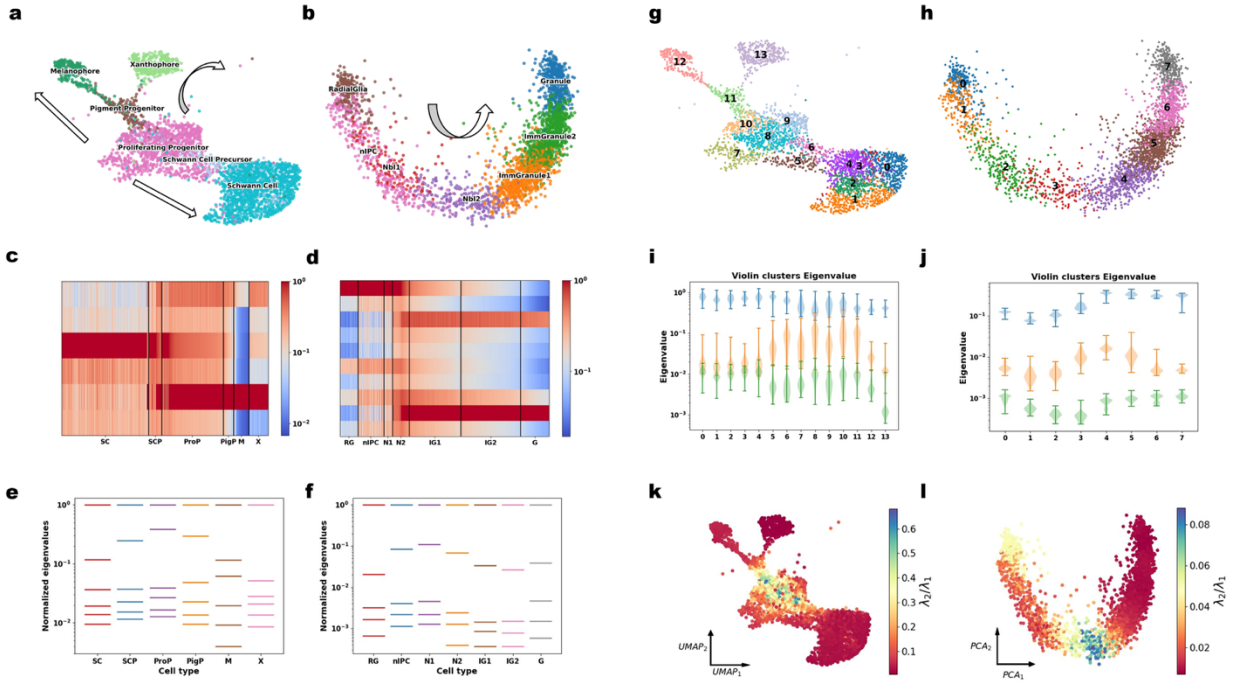

Figure 2. Spectrum analysis of Fisher information matrix.

(a)-(b) Datasets overview. The zebrafish pigmentation is a CST process involves differentiation of multiple lineages (a). For the dentate gyrus neurogenesis, the single lineage differential from radial glia cell to granule cell are focused for comparison with multi-lineage (b).

(c)-(d) The heatmap of single cell's FIM eigen value reveals the difference between cell types in zebrafish pigmentation(c) and dentate gyrus neurogenesis (d).

(e)-(f) Averaged eigen value spectrum of FIM in each cell type. The bar represents eigen value of averaged single cell in each cell type in Zebrafish pigmentation (c) and dentate gyrus. All eigenvalues are normalized by the first largest eigenvalue. The spectrum reveals the sloppiness of single cell.

(g)-(h)PAGA cluster of zebrafish pigmentation(g) and dentate gyrus(h).

(i)-(j) Violin plot of eigen value distribution of FIM in each cluster in zebrafish pigmentation(i) and dentate gyrus neurogenesis (j). In both data, only statistics on the first three largest eigen values are ploted. In each cluster, blue, orange and green violin represented the distribution of the 1st, 2nd, 3rd eigen values, respectively. These values were not normalized. The red circles marked the regions where the gap between the 1st largest eigen value and the 2nd largest eigen value become smaller.

(k)-(l) Scatter plot of the ratio of the 2nd and the 1st eigenvalues in zebrafish pigmentation (k) and dentate gyrus neurogenesis (l). Color represents value of ratio.

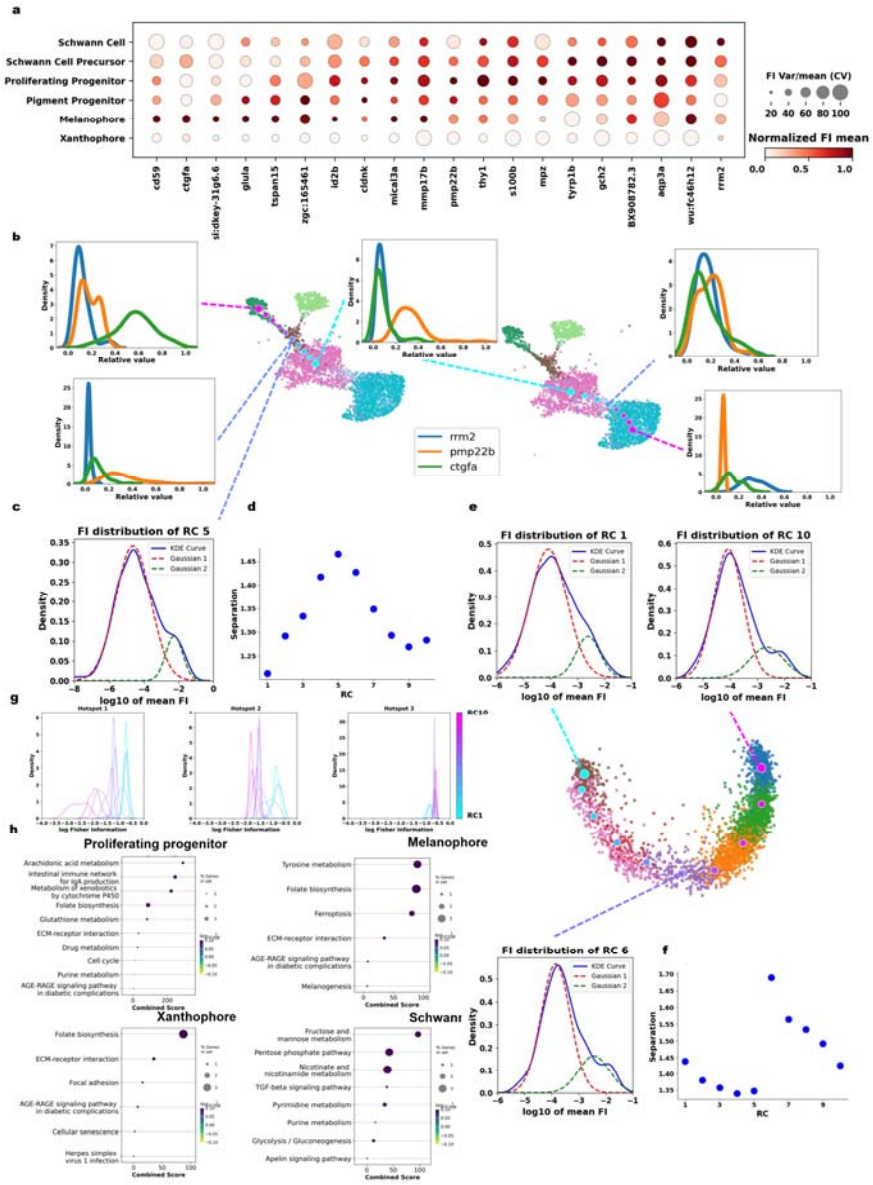

Figure 3. Gene Fisher information analyses on CST processes.

(a) Fisher information of twenty selected genes with the largest mean fisher information in different cell types of zebrafish pigmentation. The dot size represents the coefficient of variation (CV) of Fisher information in the cell type, and the color represents the mean Fisher information in the cell type, which is normalized gene-wise. We selected the 20 genes

(b) The variation of genes Fisher information along RCs. Two transition paths (left: Proliferating Progenitor → Melanophore; right: Proliferating Progenitor → Schwann Cell) was simulated (method). The Fisher information of each gene was normalized by the

maximal Fisher information of that gene across all cells. The color of scatter plot represents cell type.

(c) The gene Fisher information distribution at 5th RC from proliferating progenitor to melanophore.

(d) The separation of two peaks of the distribution varies along the RC.

(e) The gene Fisher information distribution varies along the transition of dentate gyrus. Distributions of other RCs, and of other transition paths or datasets can be found in Supplementary material.

(f) The separation of two peaks of the gene Fisher distribution varies during transition in dentate gyrus neurogenesis.

(g) The shift of Hotspot Fisher information distribution along the transition from proliferating progenitor to melanophore.

(h) The gene enrichment analysis of the top-20 genes with the largest gene Fisher information in specific cell type (proliferating progenitor, melanophore, xanthophore, and Schwann cell).

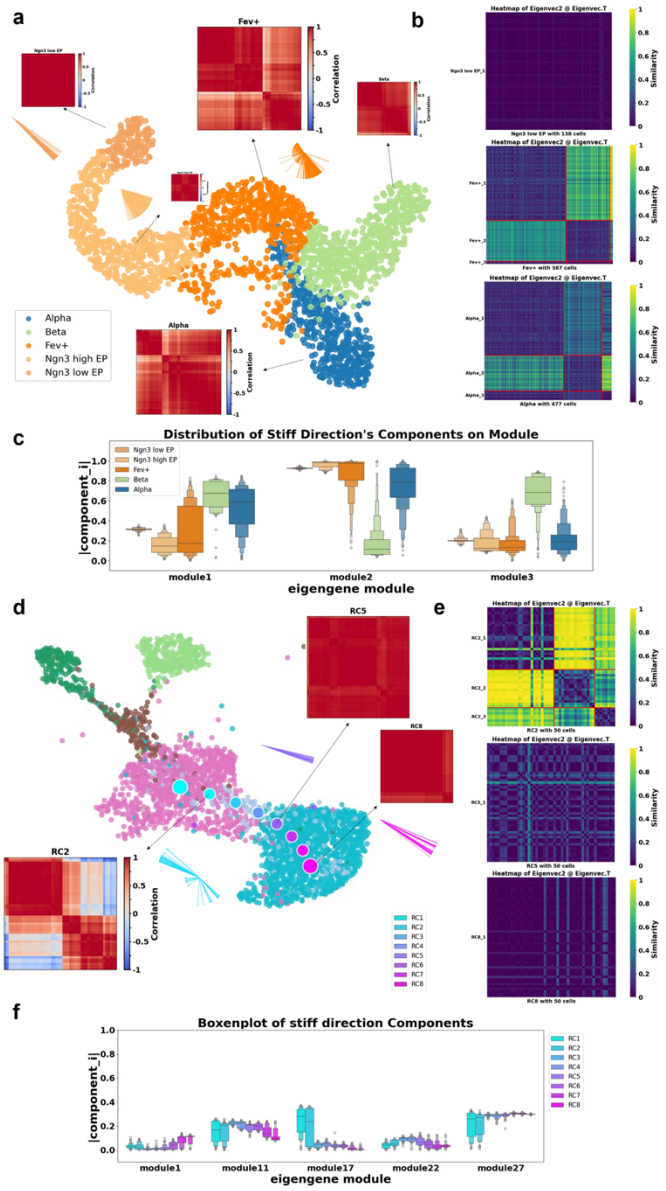

Figure 4 Relationship between critical transition and stiff direction on endocrinogenesis and zebrafish pigmentation.

(a) Distributions of stiff direction of different cell types in pancreatic endocrinogenesis data. The matrix heatmap are the correlation coefficient matrices of the stiff directions in the corresponding cell types. The inserted arrow bundles next to the matrices are visualizations of the stiff directions(methods). The length of the arrows is proportional to the proportion of the clustering results.

(b) Inner product of the second eigenvector and the first eigenvector (i.e., the stiff direction) for different cell types. The red line represents the division obtained based on the clustering results in panel (a).

(c) Distribution of each component (absolute value) of the stiff direction. The distribution of the stiff direction on each eigengene coordinate component differs in different cell types.

(d) Same as that in panel (a) except for different RCs along the transition path from proliferating progenitor to Schwann cell in zebrafish pigmentation.

(e) Same as that in panel (b) except for different RCs along the transition path from proliferating progenitor to Schwann cell in zebrafish pigmentation.

(f) Same as that in panel (c) except for different RCs along the transition path from proliferating progenitor to Schwann cell in zebrafish pigmentation.

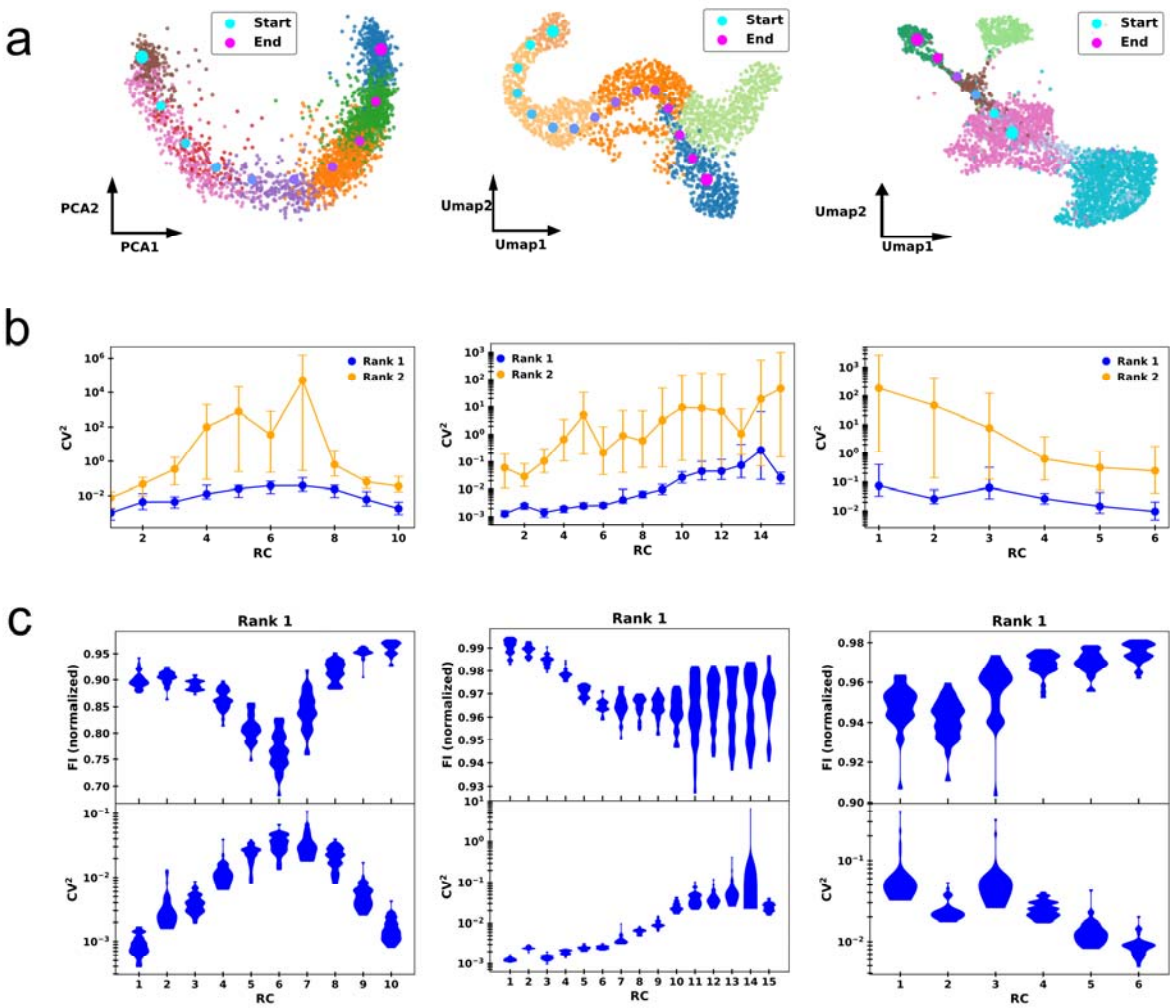

Figure 5 Fluctuation of stiff and sloppy parameters.

(a) Reaction coordinate (RC) paths for three datasets. Left: dentate gyrus dataset. Middle: alpha branch of the pancreatic endocrinogenesis dataset. Right: melanophores branch of the zebrafish pigmentation dataset.

(b) Squared coefficient of variation (CV^2) along the Reaction coordinate path for a representative stiff parameter (Rank 1, blue) and a representative sloppy parameter (Rank 2, orange) in each dataset.

(c) Along the reaction coordinate path, Fisher Information (FI) of stiff parameter is negatively correlated with their squared coefficient of variation (CV^2). The Fisher information for stiff parameter is obtained after sum-normalization across all parameters within a single cell.

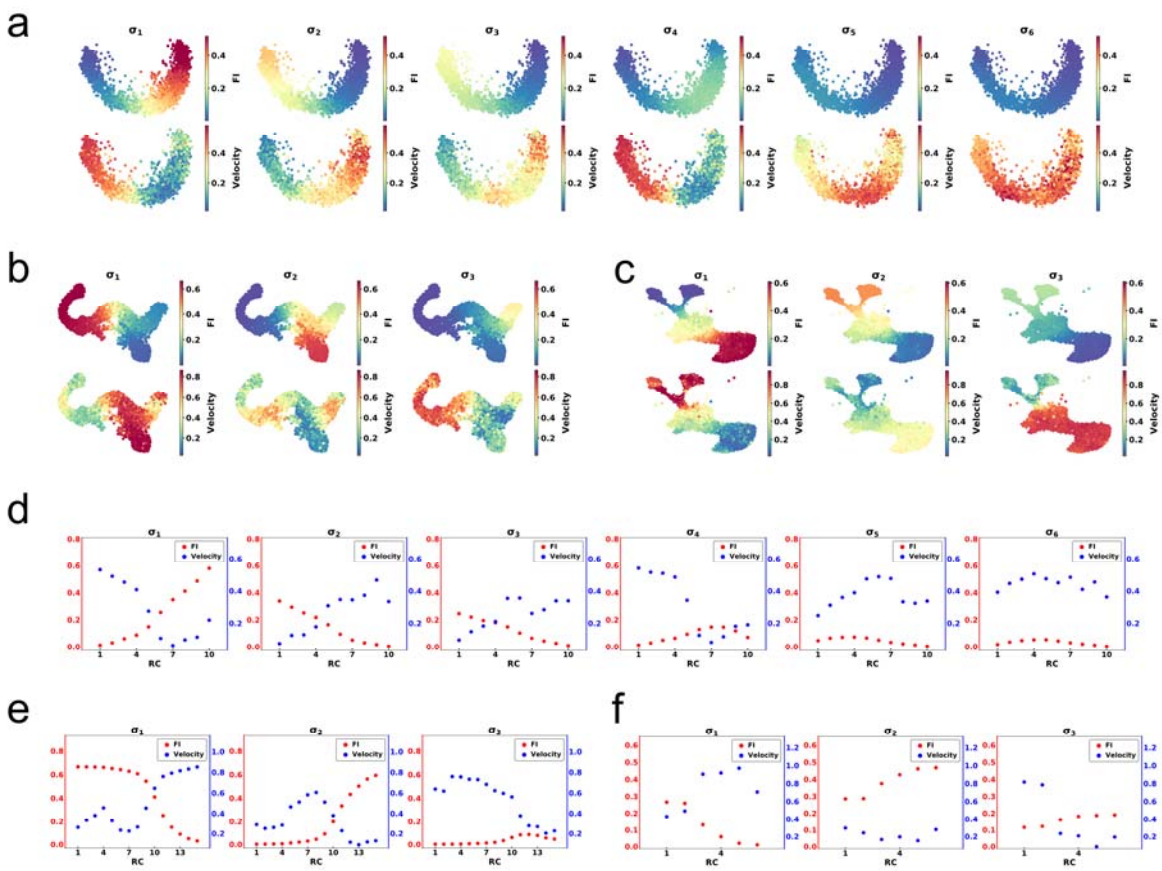

Figure 6 The relationship between parameter velocity and fisher information.

(a) Cell-wise distributions of Fisher information and parameter velocity in the dentate gyrus dataset. Each dot represents a single cell, with color indicating the value of Fisher information (top) or parameter velocity (bottom). For each cell, the Fisher information and parameter velocity of each parameter are obtained after sum-normalization across all parameters within that cell.

(b) Cell-wise distributions of Fisher information and parameter velocity in the pancreatic endocrinogenesis dataset.

(c) Cell-wise distributions of Fisher information and parameter velocity in the zebrafish pigmentation dataset.

(d) Relationship between Fisher information and parameter velocity along the reaction coordinate in the dentate gyrus dataset. At each reaction coordinate point, the Fisher information of a given parameter is computed by averaging over neighboring cells along the reaction coordinate, and the parameter velocity is computed in the same manner. Fisher information and parameter velocity are sum-normalized across parameters.

(e) Relationship between Fisher information and parameter velocity along the reaction coordinate in the α-branch of the pancreatic endocrinogenesis dataset.

(f) Relationship between Fisher information and parameter velocity along the reaction coordinate in the melanophores branch of the zebrafish pigmentation dataset.

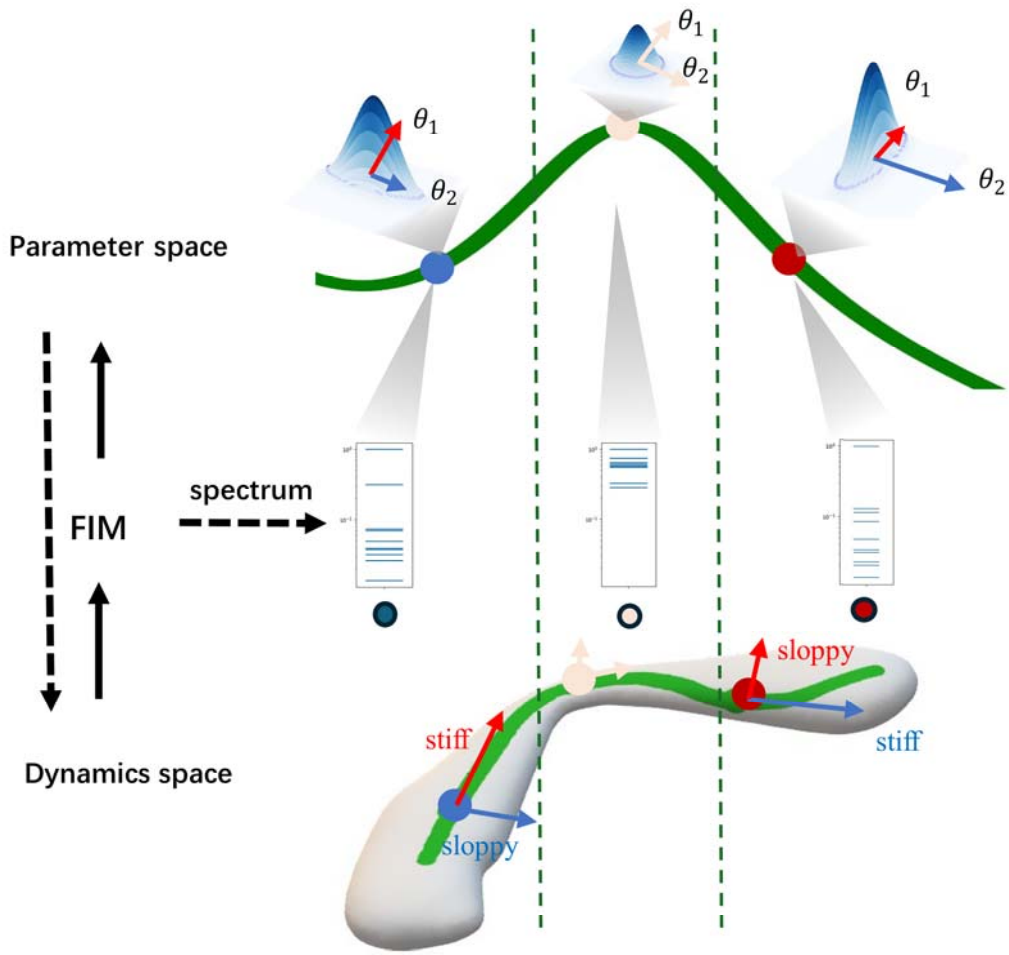

Figure 7. Analyzing CST in high-dimensional dynamics space (bottom) through mapping onto parameter space (top) by the Fisher information matrix (FIM). The two green curves in two spaces represent the same trajectory, and points with matching colors denote the same model state. The transition can be analyzed by the analyzing the spectrum of FIM. Along the path, the stiff direction switch between θ_1 (red) and θ_2 (blue). During this switching, subleading eigenvalues become comparable to the largest one, illustrating how the FIM spectrum reveals both the presence of a stiff direction and the state where multiple directions become similarly informative. As a schematic example, each point is corresponding to a (two-dimensional) Gaussian distribution in the parameter space. The arrow length at each point indicates the magnitude of the Fisher information along that direction.

Methods

Dataset and preprocessing

The single cell RNA sequencing datasets of zebrafish is available on GEO via accession GSE131136 (27). For simplicity, we focused on specific transition processes and filtered out other cell types not involved in these processes for calculation considerations. The focused differentiation process is from Proliferating Progenitor to Melanophore, Xanthophore, and Schwann Cell. Cells annotated as other cell types were removed.

The dentate gyrus neurogenesis is obtained from the GEO website with accession number GSE95753 (28). In this data, we first analyzed the single-lineage CST process from radial glia cell to mature granule cell for comparison with multiple-lineage CST processes like zebrafish pigmentation. We also analyzed the multiple lineage process including branch of differentiation from radial glia cell to CA cells.

The pancreatic endocrinogenesis data is obtained from GSE132188 (34). In this dataset, we includes both branches of glucagon-producing α-cells and β-cells.

Gaussian embedding

Gaussian embedding is a learning method for graph embedding problems and its output is a multivariate Gaussian distribution parameter (Expectations and Variances in all dimensions) for each node. A neural network is trained on the sampled triplets which contain the neighboring information of nodes by minimizing an energy-based ranking loss ($\mathcal{L}$):

$$\mathcal{L} = \sum_{i} \sum_{k<l} \sum_{j_k \in N_{ik}} \sum_{j_l \in N_{il}} (E_{ij_k}^2 + \exp(-E_{ij_l}^2))$$

where N_{ik} represents the set of nodes j_k that the length of shortest paths on the graph between node i and node j_k equal k. The energy E_{ij} represents the Fisher distance between nodes i and j.

Eigenvalue spectrum of FIM

For probability distribution with parameter θ, its FIM is defined as:

$$G(\theta) = \mathbb{E}[\frac{\partial \log p(x;\theta)}{\partial \theta}\left(\frac{\partial \log p(x;\theta)}{\partial \theta}\right)^T], \tilde{G}(\lambda) = \frac{\partial \theta}{\partial \lambda} G(\theta) \left(\frac{\partial \theta}{\partial \lambda}\right)^T$$

Where $p(x;\theta)$ is probability density function and $\tilde{G}(\lambda)$ is the FIM in another parameter λ computed through coordinate transformation from parameter θ to parameter λ. Thus, we can observe the spectrum of FIM's eigenvalue in different spaces.

In (μ,σ) space, the Fisher information matrices are diagonal. Thus, the eigenvalues are just diagonal entries.

We trained a neural network to learn the coordinate transformation from other coordinate systems to (μ,σ) space by using the auto-gradient of the neural network. In PCA, eigengene, Hotspot or other coordinate systems, we applied symmetric eigen decomposition to compute eigenvalues and eigenvectors. Because FIM is regarded as a metric matrix, the scale of its eigenvalues indicates how fast the distribution changes.

Transition path analysis

To better illustrate the variation of Fisher information during the transition process, we simulated transition trajectories on each scRNA-seq data. The simulation is performed with a transition kernel defined on the KNN graph. And we applied soft DTW algorithm to obtain a smooth average transition path.

We used cell-cell transition matrix provided by scVelo package as transition kernel (35).

$$\tilde{\pi}_{ij} = \frac{1}{z_i}\exp\left(\pi_{ij}/\sigma\right)$$

$$\pi_{ij} = cos < x_j - x_i, v_i >$$

Here, x_i represents cell i, v_i represents the RNA velocity of cell i. The cosine similarities between potential cell state transitions and RNA velocities π_{ij} were computed. It measured how well the potential transition matches the velocity. The transition probability $\tilde{\pi}_{ij}$ was then computed by applying an exp kernel.

When simulating trajectories, we first applied PAGA or used cell type annotation to split cells into several clusters and specified a starting cluster and an ending cluster. Then, we calculated the average cell of the starting cluster and selected the 200 cells nearest to that average cell as the starting cells to generate 200 trajectories. Each trajectory terminated after sticking in the ending

cluster for 10 steps. Finally, we used random walk paths with length less than 200 for soft DTW averaging.

After soft DTW averaging, we got an average transition path. Generally, many nodes along the transition path tended to gather around the starting and ending clusters. For better visualization, we further found the nearest cell in PCA space for each node on the path, and averaged nodes with same nearest cell into one.

Given a transition path discretized by r RCs, we separated the cells into r Voronoi grids by finding the nearest RC for each cell. The Fisher information of the ith RC was defined as the mean Fisher information of cell in the ith grid. The projected velocity along path was also defined in this way. The standard deviation and coefficient of variation of projected velocity along the path was defined as the std and CV of projected velocity in each cluster.

Gene Fisher information

Given Fisher information metrics in (μ, σ) space, we pulled it back to gene expression space.

$$g_{\alpha\beta} = g_{ij} \frac{\partial \theta^i}{\partial x^\alpha} \frac{\partial \theta^j}{\partial x^\beta}$$

where x^α denoted the α-element of the gene expression vector, θ^i denoted the i-element of the latent state vector in (μ, σ) space. The diagonal element $g_{\alpha\alpha}$ is defined as the gene Fisher information of the gene α.

We trained a simple MLP to fit the map from gene expression space to (μ, σ) space. The Jacobian was obtained by automatic differentiation of MLP.

We selected the top 20 genes with the highest average Fisher information across all cells for dot plot visualization. To further discuss the variation of gene Fisher information, we then selected 3 genes with different variation behavior from the 20 genes. For each selected gene, we computed its Fisher information in all cells, and normalized by its maximal Fisher information along all cells to get a relative value. The distribution of the relative Fisher information in each cell cluster or cell type was fitted by KDE (Kernel Density Estimation).

We plotted the distribution of genes' log Fisher information of each RC. The log Fisher information of gene G at each RC was defined as the mean log Fisher information of gene G over the 50-nearest cells of the RC. The distribution of the log Fisher information of each RC was defined as the distribution of log Fisher information of all genes.

We further measured the separation of the two peaks of a bimodal distribution via 4 measurements, namely, separation, Wasserstein distance, Fisher distance, and Gini coefficient, which are defined as following:

We fitted the distribution by 2 components Gaussian Mixture Model (2-GMM), and calculated the t-test distance between the 2 Gaussian components. Denote the 2 components as $\mathcal{N}(\mu_1, {\sigma_1}^2), \mathcal{N}(\mu_2, {\sigma_2}^2)$, we defined the separation as t-test distance between them, and calculated the Wasserstein distance and Fisher distance between the 2 components.

$$separation = \frac{|\mu_1 - \mu_2|}{\sqrt{\sigma_1^2 + \sigma_2^2}}$$

$$Wasserstein\ distance = \sqrt{(\mu_1 - \mu_2)^2 + (\sigma_1 - \sigma_2)^2}$$

$$Fisher\ distance = \sqrt{2\ln\frac{\sqrt{\frac{(\mu_1 - \mu_2)^2}{2} + (\sigma_1 + \sigma_2)^2} + \sqrt{\frac{(\mu_1 - \mu_2)^2}{2} + (\sigma_1 - \sigma_2)^2}}{\sqrt{\frac{(\mu_1 - \mu_2)^2}{2} + (\sigma_1 + \sigma_2)^2} - \sqrt{\frac{(\mu_1 - \mu_2)^2}{2} + (\sigma_1 - \sigma_2)^2}}}$$

We also use Gini coefficient to measure the dispersion of the distribution.

$$Gini\ coefficient = \frac{\sum_{i=1}^{n}\sum_{j=1}^{n}|x_i - x_j|}{2\mathrm{n}\sum_{k=1}^{n} x_k}$$

where x_i are $i.i.d$ samples from a distribution supported on positive real numbers. Note that the distributions of log Fisher information are supported on negative real numbers, thus we timed data with -1 before calculating the Gini coefficients.

Stiff direction analysis

Stiff direction is defined to be the eigenvector of FIM corresponding to the largest eigenvalue. To calculate the stiff direction of a single cell, we need to diagonalize the FIM. However, there is an

ambiguity in this definition: the reverse direction of a stiff direction is still a stiff direction. This cause troubles when considering the distribution of stiff directions among a collection of cells.

We use eigenvectors of Fisher information matrix in PCA space for stiff direction analysis. To focus on the dominant direction, we only considered the first eigenvector.

Since eigenvectors have the ambiguity of sign, we use RNA velocity for alignment. In each cell type, we computed the mean RNA velocity. For each cell in that cell type, we chose the direction of eigenvector leading to non-negative inner product of the eigenvector and the mean velocity. After alignment, we applied PCA to eigenvectors in each cell type. The first two PCs were used for 2D visualization. When computing correlation matrix, we used the original direction vectors.

Gurobi solver

For each cell, we select the eigenvector corresponding to the largest eigenvalue of its metric matrix. Within each cell type, these eigenvectors are then clustered using the cosine distance between vectors. However, since the direction of an eigenvector can be reversed (i.e., multiplied by -1) without altering its validity, this operation can affect the calculated distance between vectors, thereby influencing the clustering outcome. To address this, we determine the optimal orientation of each eigenvector by solving the following optimization problem:

$$\min_{c_i \in \pm 1} -\sum_{i,j} c_i c_j v_i^T v_j$$

Where v_i denotes the eigenvectors. Since the vectors are unit vectors, we minimize their negative correlation in the optimization; is an indicator for determining the direction of each vector.

This formulation constitutes a binary quadratic optimization (BQO) problem. We employ the Gurobi solver to obtain the solution, utilizing the commonly used branch-and-bound algorithm from integer programming.

To measure the dispersion of stiff direction distribution along transition path, we computed the coefficient of variation (CV) and total variance. Stiff direction vectors could be simply viewed as points distributed in high dimensional space. In each coordinate direction, the CV of the 1-dim distribution was computed. It measured the dispersion of stiff directions distribution in that

direction. To measure the total dispersion, we multiplied the CVs in each direction. This product measured the dispersion of the stiff direction distribution. The larger, the dispersive. We computed the covariance matrix of stiff directions in each cluster, and used the total variance i.e. the trace of the covariance matrix to measure the dispersion of the stiff direction distribution. The larger, the dispersive.

Coefficient of variation of parameters

The coefficient of variation (CV) is a relative statistic that measures the degree of data variability. It is used to compare the variability of sample data with different means and is defined as the ratio of the standard deviation to its mean:

$$CV = \frac{\sigma}{\mu}$$

The parameters considered here represent the coordinates defined by the eigenvectors of the Fisher Information Matrix in PCA space, obtained as follows:

$$FIM_{pca} = Q\Lambda Q^{-1}$$

$$\lambda = Q^T\ PCA$$

where, Q is an orthogonal matrix, whose columns are the eigenvectors of FIM_{pca}, and Λ is a diagonal matrix containing the corresponding eigenvalues. Notably, Λ is also the Fisher information matrix of the parameter λ. So, parameters corresponding to large eigenvalues are therefore stiff, while those associated with small eigenvalues are sloppy. The derivation is as follows:

$$Q^T = Q^{-1} \Leftrightarrow QQ^T = I$$

$$PCA = Q\lambda$$

$$\frac{\partial PCA}{\partial \lambda} = Q^T$$

$$FIM_\lambda = \frac{\partial PCA}{\partial \lambda} FIM_{pca} \left(\frac{\partial PCA}{\partial \lambda}\right)^T = Q^T FIM_{pca} (Q^T)^T = Q^T Q\Lambda Q^{-1}\mathrm{Q} = \Lambda$$

For each reaction coordinate point, we select the 30 nearest neighboring cells as sample to calculate CV^2. we assume that cells located close to a reaction coordinate point belong to the same cell state and are governed by a similar set of parameters. The distance is calculated in the corresponding single-cell RNA sequencing data data's Clustering and Dimension Reduction space, specifically, using the 2D leading principal components (PCs) distance for dentate gyrus dataset, and UMAP distance for pancreatic endocrinogenesis and zebrafish pigmentation dataset.

We compute CV^2 for parameters at each reaction coordinate point following the same idea used for computing *projection change* in *Sloppiness in Spontaneously Active Neuronal Networks.* As an example, the CV^2 of the stiffest parameter λ_1 at the first reaction coordinate point RC_1 is computed as follows:

$$\mu_{RC_1,i} = \frac{1}{N}\sum_{j}^{N}(q_{cell\ i,\ 1}{}^{T}\ PCA_{\ cell\ j})$$

$$s^2_{RC_1,i} = \frac{1}{N-1}\sum_{j}^{N}(q_{cell\ i,\ 1}{}^{T}\ PCA_{\ cell\ j} - \mu_{RC_1,i})^2$$

$$CV^2_{RC_1} = \frac{1}{N}\sum_{i}^{N}\frac{s^2_{RC_1,i}}{\mu_{RC_1,i}}$$

Where, $q_{cell\ i,\ 1}$ denotes the eigenvector corresponding to the largest eigenvalue of FIM_{pca} for $cell\ i$, $PCA_{\ cell\ j}$ denotes the PCA coordinates of neighboring $cell\ j$, and N is the number of neighboring cells, here $N = 30$.

Parameter velocity

Gaussian embedding maps cells from the gene expression space to a manifold space. This manifold is equipped with the Fisher Information Metric (FIM) as its metric, and the coordinates on the manifold are given by the parameters of the probability density function. In our setting, the probability density function is chosen to be a Gaussian distribution, whose parameters are the mean μ and the standard deviation σ.We refer to this manifold as the (μ,σ) space. In this space, the velocity of the parameter θ, denoted as v_θ, is defined and computed as follows:

$$v_\theta = \frac{d\theta}{dt} = \frac{dx_i}{dt}\frac{\partial\theta}{\partial x_i} = \tilde{v}_i \frac{\partial\theta}{\partial x_i}$$

Where $\frac{\partial\theta}{\partial x_i}$ is calculated using Pytorch autograd function numerically from Gaussian embedding model.

References

1. Goldberg AD, Allis CD, Bernstein E. Epigenetics: A Landscape Takes Shape. Cell. 2007;128(4):635-8.
2. Ye Z, Sarkar CA. Towards a Quantitative Understanding of Cell Identity. Trends Cell Biol. 2018;28(12):1030-48.
3. Jin S, MacLean AL, Peng T, Nie Q. scEpath: energy landscape-based inference of transition probabilities and cellular trajectories from single-cell transcriptomic data. Bioinformatics. 2018;34(12):2077-86.
4. Shi J, Teschendorff AE, Chen W, Chen L, Li T. Quantifying Waddington's epigenetic landscape: a comparison of single-cell potency measures. Briefings in Bioinformatics. 2018;21(1):248-61.
5. Teschendorff AE, Enver T. Single-cell entropy for accurate estimation of differentiation potency from a cell's transcriptome. Nature Communications. 2017;8(1):15599.
6. Wang S, Sontag ED, Lauffenburger DA. What cannot be seen correctly in 2D visualizations of single-cell 'omics data? Cell Systems. 2023;14(9):723-31.
7. Huang M, Ying J, Wang Y, Zhou H, Zhang L, Wang W. Geometric Quantification of Cell Phenotype Transition Manifolds with Information Geometry. bioRxiv. 2024:2023.12.28.573500.
8. Transtrum MK, Machta BB, Brown KS, Daniels BC, Myers CR, Sethna JP. Perspective: Sloppiness and emergent theories in physics, biology, and beyond. The Journal of Chemical Physics. 2015;143(1).
9. Quinn KN, Abbott MC, Transtrum MK, Machta BB, Sethna JP. Information geometry for multiparameter models: new perspectives on the origin of simplicity. Reports on Progress in Physics. 2023;86(3):035901.
10. Machta BB, Chachra R, Transtrum MK, Sethna JP. Parameter Space Compression Underlies Emergent Theories and Predictive Models. Science. 2013;342(6158):604-7.
11. Transtrum MK, Machta BB, Sethna JP. Why are Nonlinear Fits to Data so Challenging? Physical Review Letters. 2010;104(6):060201.
12. Quinn KN, Wilber H, Townsend A, Sethna JP. Chebyshev Approximation and the Global Geometry of Model Predictions. Physical Review Letters. 2019;122(15):158302.
13. Agozzino L, Balázsi G, Wang J, Dill KA. How Do Cells Adapt? Stories Told in Landscapes. Annu Rev Chem Biomol Eng. 2020;11:155-82.
14. DiFrisco J, Jaeger J. Genetic Causation in Complex Regulatory Systems: An Integrative Dynamic Perspective. BioEssays. 2020;42(6):1900226.
15. Kim Y, Kim T-K, Kim Y, Yoo J, You S, Lee I, et al. Principal network analysis: identification of subnetworks representing major dynamics using gene expression data. Bioinformatics. 2010;27(3):391-8.
16. Wang W, Ni K, Poe D, Xing J. Transiently Increased Coordination in Gene Regulation During Cell Phenotypic Transitions. PRX Life. 2024;2(4):043009.
17. Hennig MH. The sloppy relationship between neural circuit structure and function. The Journal of Physiology. 2023;601(15):3025-35.
18. Daniels BC, Chen Y-J, Sethna JP, Gutenkunst RN, Myers CR. Sloppiness, robustness, and evolvability in systems biology. Current Opinion in Biotechnology. 2008;19(4):389-95.
19. Panas D, Amin H, Maccione A, Muthmann O, van Rossum M, Berdondini L, et al. Sloppiness in spontaneously active neuronal networks. J Neurosci. 2015;35(22):8480-92.

20. Ponce-Alvarez A, Mochol G, Hermoso-Mendizabal A, de la Rocha J, Deco G. Cortical state transitions and stimulus response evolve along stiff and sloppy parameter dimensions, respectively. eLife. 2020;9:e53268.
21. Gutenkunst RN, Waterfall JJ, Casey FP, Brown KS, Myers CR, Sethna JP. Universally Sloppy Parameter Sensitivities in Systems Biology Models. PLOS Computational Biology. 2007;3(10):e189.
22. Crooks GE. Measuring Thermodynamic Length. Physical Review Letters. 2007;99(10):100602.
23. Kim EJ, Lee U, Heseltine J, Hollerbach R. Geometric structure and geodesic in a solvable model of nonequilibrium process. Phys Rev E. 2016;93(6):062127.
24. Qiu X, Zhang Y, Martin-Rufino JD, Weng C, Hosseinzadeh S, Yang D, et al. Mapping transcriptomic vector fields of single cells. Cell. 2022;185(4):690-711.e45.
25. Wang J. Landscape and flux theory of non-equilibrium dynamical systems with application to biology. Advances in Physics. 2015;64:1 - 137.
26. Zhu L, Yang S, Zhang K, Wang H, Fang X, Wang J. Uncovering underlying physical principles and driving forces of cell differentiation and reprogramming from single-cell transcriptomics. Proceedings of the National Academy of Sciences. 2024;121(34):e2401540121.
27. Saunders LM, Mishra AK, Aman AJ, Lewis VM, Toomey MB, Packer JS, et al. Thyroid hormone regulates distinct paths to maturation in pigment cell lineages. eLife. 2019;8:e45181.
28. Hochgerner H, Zeisel A, Lönnerberg P, Linnarsson S. Conserved properties of dentate gyrus neurogenesis across postnatal development revealed by single-cell RNA sequencing. Nature Neuroscience. 2018;21(2):290-9.
29. Pinele J, Strapasson JE, Costa SIR. The Fisher–Rao Distance between Multivariate Normal Distributions: Special Cases, Bounds and Applications. Entropy. 2020;22(4):404.
30. Costa SIR, Santos SA, Strapasson JE. Fisher information distance: A geometrical reading. Discrete Applied Mathematics. 2015;197:59-69.
31. E W, Vanden-Eijnden E. Transition-path theory and path-finding algorithms for the study of rare events. Annu Rev Phys Chem. 2010;61:391-420.
32. Haghverdi L, Büttner M, Wolf FA, Buettner F, Theis FJ. Diffusion pseudotime robustly reconstructs lineage branching. Nature Methods. 2016;13(10):845-8.
33. Setty M, Kiseliovas V, Levine J, Gayoso A, Mazutis L, Pe’er D. Characterization of cell fate probabilities in single-cell data with Palantir. Nature Biotechnology. 2019;37(4):451-60.
34. Bastidas-Ponce A, Tritschler S, Dony L, Scheibner K, Tarquis-Medina M, Salinno C, et al. Comprehensive single cell mRNA profiling reveals a detailed roadmap for pancreatic endocrinogenesis. Development. 2019;146(12).
35. Bergen V, Lange M, Peidli S, Wolf FA, Theis FJ. Generalizing RNA velocity to transient cell states through dynamical modeling. Nature Biotechnology. 2020;38(12):1408-14.